Heliyon 10 (2024) e35479

Contents lists available at ScienceDirect

Heliyon

journal homepage: www.cell.com/heliyon

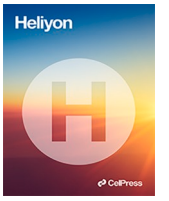

Research article

Synthesis, light-controlled antibacterial and anti-tumor activities of *Ginkgo biloba* leaves polyprenols-based polypyridine metal complexes

Changwei Zhang [a,b,*], Hua Yuan [a,b], Hong Shen [a,b], Jianzhong Ye [a,b], Chengzhang Wang [a,b,**]

[a] *Institute of Chemical Industry of Forest Products, CAF, Nanjing, 210042, Jiangsu, China*
[b] *Co-Innovation Center of Efficient Processing and Utilization of Forest Resources, Nanjing Forestry University, Nanjing, 210042, Jiangsu, China*

ARTICLE INFO

Keywords:
Polyprenols
Functional modification
Light-responsive
Biological activity
Mechanism

ABSTRACT

In this study, *Ginkgo biloba* leave polyprenols (GBP) and polypyridine metal complex were individually utilized as functional ligand and main ligand, four kinds of novel GBP-based polypyridine metal complexes were successfully synthesized and their cell absorption capacity, light-dark stability, photodissociation efficiency, ROS production capacity, light-controlled antibacterial and anti-tumor activities as well as mechanisms were systematically investigated by ultraviolet visible spectrophotometer (UV–vis), confocal laser scanning microscope (CLSM), gel electrophoresis (GE), scanning electron microscope (SEM), oxford cup method, MTT method etc. The lipid water distribution coefficients of complex 1, 2 and 4 were all within the range of 0~3, demonstrating their better cell absorption capacity and more competitive bioavailability potentiality compared with GBP. All of the synthesized complexes possessed excellent stability in a dark environment, and could conduct ligand dissociation under the condition of visible light irradiation except complex 1. In which, complex 2 and complex 4 were able to achieve degradation rates of 37.9 % and 54.4 % within 5 min, separately. In addition, complex 2 and complex 4 exhibited superior inhibitory activities on the HN-3 tumor cells on account of their stronger ROS production capacity. Moreover, the constricted expression of BCL-2 and NF-kB p-p65, especially the promoted expression of BAX may be one of the root cause. The four synthesized complexes had preferable inhibition effects against *S. aureus* under the condition of visible light irradiation in contrast to darkness, in which complex 4 was the best and its MIC and MBC values were 6.25 and 12.5 μg/mL, respectively. The antibacterial mechanism of the complex 4 may be in relation to the synergistic effect of multiple factors, including leakage of bacterial inclusion, change of cell membrane permeability and disruption of cell wall etc. All of the above generalized researches will pave a way for the high-value development and application of GBP-based functional products.

* Corresponding author. Institute of Chemical Industry of Forest Products, CAF, Nanjing, 210042, Jiangsu, China.
** Corresponding author. Institute of Chemical Industry of Forest Products, CAF, Nanjing, 210042, Jiangsu, China.
E-mail address: zhangcwlhs@sina.com (C. Zhang).

https://doi.org/10.1016/j.heliyon.2024.e35479
Received 20 December 2023; Received in revised form 29 July 2024; Accepted 29 July 2024
Available online 31 July 2024

1. Introduction

Ginkgo biloba is a unique plant with abundant forest resources in China, and its extract (GBE) that mainly composed of flavonoids and lactones possesses a high global sales market. However, due to the impact of "acid water extraction incident in 2015″, resulting in the entire *Ginkgo biloba* industry encountered a "downturn period". Therefore, developing new GBE alternative products becomes a major demand for the *Ginkgo biloba* industry. In recent years, polyprenols as a new active lipid ingredient with various isoprene units in the *Ginkgo biloba* leave, has been favored by researchers because of its structural similarity to the dolichol that involved in human glycoprotein synthesis [1]. It was reported that *Ginkgo biloba* leave polyprenols (GBP) possessed inhibition effect on the *Salmonella enterica*, *Staphylococcus aureus*, *Aspergillus niger*, *Escherichia coli*, *Bacillus subtilis*, Hepatocellular carcinoma, MHCC97H cell etc., broad-spectrum antibacterial and antitumor activities made it highly promising in the field of functional products [2–4]. Thus, realizing the development and application of GBP-based functional products will become an important breakthrough in term of revitalizing *Ginkgo biloba* industry. However, low bioavailability, relatively weak biological activity when used alone, a lack of targeting and easy to produce drug resistance have limited its development and application of functional products.

Nowadays, the main methods to improve the bioavailability and biological activities of GBP are chemical and physical modifications, as well as the utilization of other active ingredients in combination. Zhou et al. synthesized GBP derivatives through esterification reaction, and found that their antibacterial activities were higher than GBP [5]. Zhang et al. prepared a GBP liposomal gel by film dispersion method, and discovered that both the bioavailability and antibacterial effect of the GBP liposomal gel were improved [6]. Yuan et al. designed a GBP-poly (β-amino ester)-galactose by Michael addition reaction, and revealed that its inhibitory activity against HepG2 tumor cell was enhanced when utilized in conjunction with DOX [7]. Bioavailability, biological activity, targeting and drug resistance are key factors affecting the development and application of efficient GBP-based functional products. Although the above methods can reform the bioavailability and biological activities of GBP to a certain extent, they still cannot solve its targeting and drug resistance issues. Therefore, seeking an generalized strategy that can simultaneously overcome the above problems is particularly crucial.

The design and synthesis of polypyridine metal complex is always a research hotspot in recent years due to its rich and adjustable hydrophilicity, easy cell absorption, fast metabolism, low toxicity, low susceptibility to drug resistance and targeted synergistic effects etc [8]. Traditional polypyridine metal complex was made up of main ligand and non-activity functional ligand. Currently, introducing bioactive molecules that are able to be used as departing functional ligands into polypyridine metal complexes, thereby realizing simultaneous release of dihydrate with cross-linked biomolecule (DNA) function and bioactive molecules after light irradiation become a trend. Sgambelone et al. brought in protease inhibitors and small molecule active substance as dissociative functional ligands on polypyridine metal complexes, achieving synergistic effects by covalent binding of ruthenium pyridine moieties to DNA and the inherent activity of biomolecules under visible light irradiation [9]. Polypyridine metal complex is positively charged, and isopentenyl structure in GBP has the ability to increase positive charge density of the polypyridine metal complex and then enhance its targeted adsorption on the surface of negatively charged bacteria and tumor cell etc [10].

Cell absorption capacity, light-dark stability, photodissociation efficiency, ROS production capacity and light-controlled activity are key factors that affecting the bioavailability, synergistic effect, drug resistance and application value of polypyridine metal complexes [11–14]. In addition, hydrophobicity of functional ligand, as well as hydrophily and electron-withdrawing ability of main ligand, are the main factors that influencing physical and chemical properties of polypyridine metal complexes. Barton et al. found that functional ligands with strong hydrophobicity could significantly enhance the cellular absorption capacity of polypyridine metal complexes [15]. Zheng et al. revealed that introducing substituents with stronger electron withdrawing effects on 2,2-bipyridine can improve the light-dark stability of the complex [16]. Lam et al. proved that polypyridine metal complexes exhibited significant differences in their ROS production ability with different hydrophilic and electron withdrawing groups on the pyridine ring [17]. Mariappan et al. proclaimed that the strength of light-controlled activity was related to the electron withdrawing groups on the pyridine ring of the polypyridine metal complex [18].

To sum up, GBP with isopentenyl structure, strong hydrophobicity and broad-spectrum antibacterial and antitumor activities is an advantageous model for the functional ligand of polypyridine metal complex. Based on this, the research ideas proposed in this study were as follows: GBP was adopted as raw material, a series of GBP-based polypyridine metal complexes were synthesized by coordination reaction etc.; The synthesized complexes possessed positive charge and could selectively adsorb on the surface of bacteria or tumor cells with negative charge; When the complexes entered interior of bacterial or tumor cells, they can simultaneously release metal polypyridine moiety, GBP functional ligand and ROS under visible light irradiation, thereby achieving synergistic effect and reversing drug resistance. These researches will present excellent application prospects for GBP in industries such as tolerable antitumor drugs, antibacterial infection cosmetics, food preservatives, and antibacterial feed additives etc.

2. Materials and methods

2.1. Chemical reagents and samples

Staphylococcus aureus (*S. aureus*) CGMCC 1.89 was obtained from China General Microbiological Culture Collection Center. GBP (≥98 %) was prepared from our laboratory. Diphenylpyrimidine (97 %), iridium trichloride hydrochloride hydrate (>99.9 %), ammonium hexafluorophosphate (99.5 %), 2-pyridine-3-quinoline-4-carboxylic acid (95 %), dichloromethane (99.5 %), anhydrous sodium sulfate, alumina (99.8 %), anhydrous ethanol, polyvinyl alcohol, ethyl acetate (99.5 %), diphenyl quinoxaline (98 %), indigo (97 %), sodium hydroxide (97 %), 2-(pyridin-2-yl) quinoline-4-carboxylic acid, methanol (99.5 %), n-octanol (99.9 %), dimethyl

sulfoxide (99.5 %), dimercaptosuccinic acid (≥98 %), phosphate buffer solution, thiazolyl blue, glucose (98 %), 4-dimethylaminopyridine (99 %), silver trifluoromethanesulfonate (97 %), 1,3-dicyclohexylcarbodiimide (99 %), diphenylquinoline (≥99 %), 2′,7′-dichlorohydrofluorescein hexyl ester (≥97 %), 2-acetylpyridine (98 %), diphenylquinoxaline (98 %), 2-ethoxyethanol (≥99.8 %), Mueller-Hinton agar, NB medium and nutrient broth were all purchased from Aladdin Reagent (Shanghai) Co., Ltd. DCFH-DA fluorescent probe and HN-3 cells were got from Wuhan Pricella Biotechnology Co., Ltd.

2.2. Synthesis of GBP-based polypyridine metal complexes

Diphenylpyrimidine (0.21 g, 0.9 mmoL) and iridium trichloride hydrochloride (0.11 g, 0.3 mmoL) were weighted and put into a 100 mL of reaction flask, then a mixed solvent of 2-ethoxyethanol (9 mL) and water (3 mL) was added, and the reaction was conducted at 110 °C under nitrogen protection for 24 h to obtain iridium dichloride bridge compound. Dissolving the iridium dichloride bridge compound in dichloromethane (DCM), then 2-ethoxyethanol and 2-pyridine-3-quinoline-4-carboxylic acid were added, raising the reaction temperature to 60 °C and stirring for 24 h, cooling, adding ammonium hexafluorophosphate (NH_4PF_6), pouring the reaction solution into water and extracting with DCM, washing the organic phase with water, drying with anhydrous sodium sulfate, concentrating, separating by a neutral alumina column (EtOH:DCM = 1:1), 80 mg of carboxyl substituted complex was obtained, and its yield was 25.6 %. Dissolving the carboxyl substituted complex in DCM, adding an excess of polyvinyl alcohol, 1,3-dicyclohexylcarbodiimide (DCC) and a catalytic amount of 4-dimethylaminopyridine (DMAP). The reaction was carried out for more than 72 h to gain GBP-based polypyridine metal complex 1 (reddish brown) with a yield of 13.0 % (see Fig. 1).

2-pyridine-3-quinoline-4-carboxylic acid was dissolved in DCM and poured into a 100 mL of reaction flask, then an excess of GBP, 1,3-dicyclohexylcarbodiimide and a catalytic amount of 4-dimethylaminopyridine were added. The reaction lasted for more than 72 h to achieve GBP modified pyridinoquinoline, with a yield of 35.1 %. Diphenylpyrimidine (0.21 g, 0.9 mmoL) and iridium trichloride hydrochloride (0.11 g, 0.3 mmoL) were weighted and put into a 100 mL of reaction flask, then a mixed solvent of 2-ethoxyethanol (9 mL) and water (3 mL) was added, and the reaction was performed at 110 °C under nitrogen protection for 24 h to get iridium dichloride bridge compound. Dissolving the iridium dichloride bridge compound in DCM, then GBP modified pyridinoquinoline and ethanol were added, elevating the temperature to 60 °C and stirring for 24 h, cooling and pouring the reaction solution into water, extracting with DCM and washing the organic phase with water, drying with anhydrous sodium sulfate and concentrating. Finally, a neutral alumina column (EA:DCM = 1:3) was adopted to separate, and 80 mg of GBP-based polypyridine metal complex 2 (purplish red) with a yield of 25.6 % was acquired by concentrating the eluent (see Fig. 2).

Diphenyl quinoxaline (0.25 g, 0.9 mmoL) and iridium trichloride hydrochloride (0.11 g, 0.3 mmoL) were weighted and put into a 100 mL of reaction flask, then a mixed solvent of 2-ethoxyethanol (9 mL) and water (3 mL) was added, and the reaction was executed at 110 °C under nitrogen protection for 24 h to attain iridium dichloride bridge compound. Dissolving the iridium dichloride bridge compound in DCM, then 2-pyridine-3-quinoline-4-carboxylic acid and 2-ethoxyethanol were added, increasing the temperature to 60 °C and stirring for 24 h, cooling and adding ammonium hexafluorophosphate, stirring and pouring the reaction solution into water, extracting with DCM and washing the organic phase with water, drying with anhydrous sodium sulfate, concentrating and separating by a neutral alumina column (EtOH:DCM = 1:1), 80 mg of carboxyl substituted complex with a yield of 25.6 % was got. Dissolving the carboxyl substituted complex in DCM, then an excess of polyvinyl alcohol, 1,3-dicyclohexylcarbodiimide and a catalytic amount of 4-dimethylaminopyridine were added. The reaction was implemented more than 128 h to get GBP-based polypyridine metal complex 3 (purplish red) with a yield of 11.3 % (see Fig. 3).

A mixture containing indigo (1.47 g, 10 mmoL), sodium hydroxide (0.80 g, 20 mmoL) and ethanol (20 mL) were heated at 78 °C for 1 h. Then, 2-acetylpyridine (1.21 g, 10 moL) was added after reflux and stirring for 4 h. Cooling and carefully pouring the mixture into water, 2.02 g of 2- (pyridin-2-yl) quinoline-4-carboxylic acid (Py-KL-Acid) with a yield of 80.8 % was achieved by acidating with

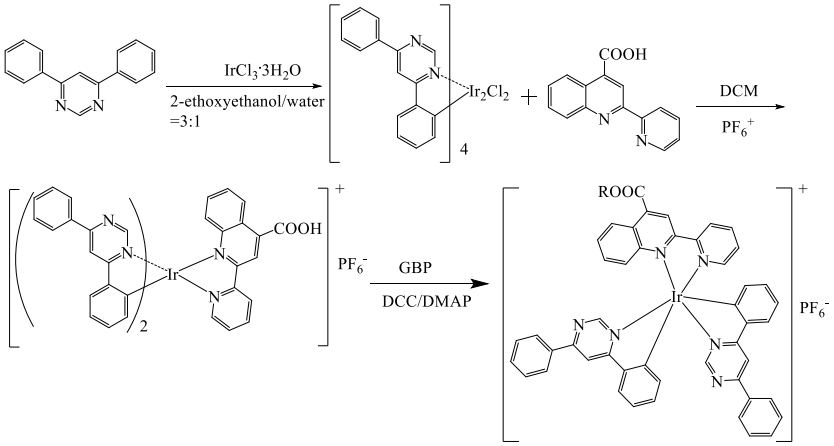

Fig. 1. Synthesis route of GBP-based polypyridine metal complex 1 (R was GBP).

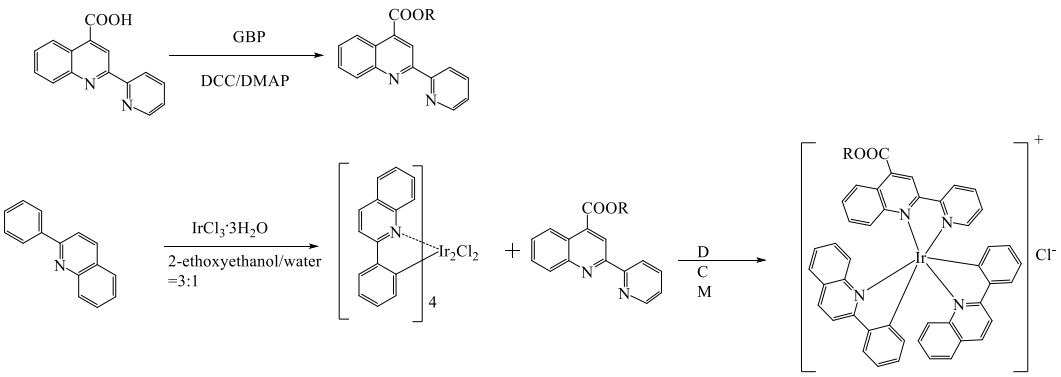

Fig. 2. Synthesis route of GBP-based polypyridine metal complex 2 (R was GBP).

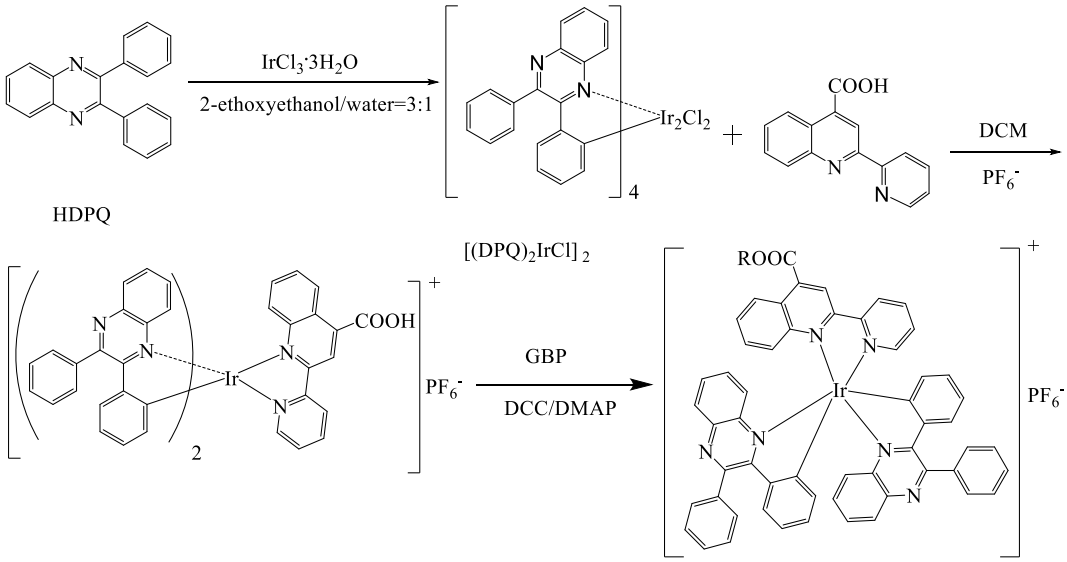

Fig. 3. Synthesis route of GBP-based polypyridine metal complex 3 (R was GBP).

hydrochloric acid and filtering. Dissolving Py-KL-Acid (0.50 g, 2 mmoL) in dry and anhydrous DCM, then excess GBP, a catalytic amount of 1,3-dicyclohexylcarbodiimide and 4-dimethylaminopyridine were added. The reaction lasted for more than 7 d. Pouring the reaction solution into water, extracting with DCM and washing the organic phase with water, drying with anhydrous sodium sulfate and concentrating, performing column chromatography (EA: PE = 1:5) separation and concentrating the eluent, 320 mg of a light yellow and oily GBP modified pyridinoquinoline with a yield of 35.6 % was obtained. Dissolving *cis*-Ru $(bpy)_2Cl_2$ (101.8 mg, 0.20 mmoL) in a mixture solution of DCM and methanol (1:1, v/v), then adding $AgSO_3CF_3$ (105 mg, 0.41 mmoL) and carrying out the reaction overnight under nitrogen protection at room temperature. The filtrate was gained by filtering and separating, then an excess of GBP modified pyridine quinoline was added into the filtrate, enhancing the temperature to 60 °C and stirring for 24 h. Adding an excess of ammonium hexafluorophosphonate and continuing the reaction overnight, cooling and pouring the reaction solution into water, extracting with DCM and washing organic phase with water, drying with anhydrous sodium sulfate and concentrating, 75 mg of GBP-based polypyridine metal complex 4 (pale yellow) with a yield of 45.2 % was achieved by a neutral alumina column (EA:DCM = 1:3) separation and concentrating the eluent (see Fig. 4).

The above prepared GBP-based polypyridine metal complexes were singly dissolved in deuterated chloroform, and analyzed by nuclear magnetic resonance spectroscopy (^{1}H NMR).

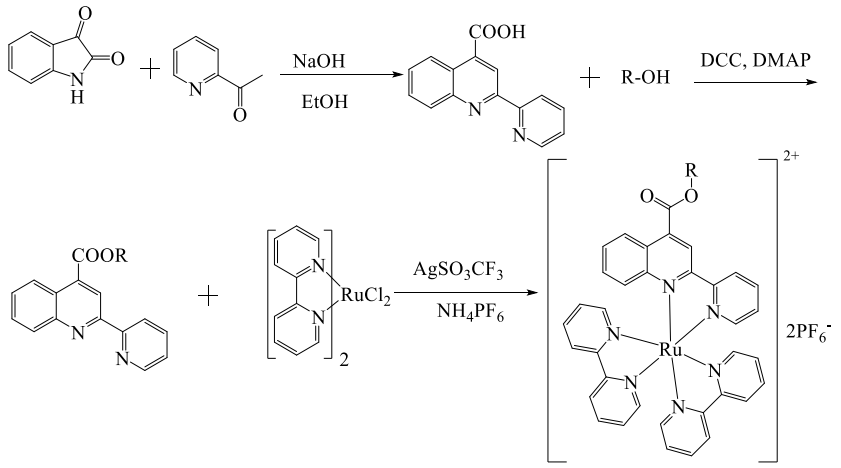

Fig. 4. Synthesis route of GBP-based polypyridine metal complex 4 (R was GBP).

2.3. Cell absorption capacity

Cell absorption capacity of the synthesized GBP-based polypyridine metal complexes were evaluated by measuring their lipid water distribution coefficients. The lipid water distribution coefficient refers to the dissolution and distribution rate of a compound in both the aqueous and lipid phases. By virtue of measuring this coefficient, the ability of a compound to penetrate the cell membrane can be reflected. The aqueous solutions of the synthesized GBP-based polypyridine metal complexes were separately added to n-octanol and sonicated for a period of time to achieve equilibrium between the two phases. After centrifugation, concentrations of GBP-based polypyridine metal complexes in the two phases were determined by absorption spectroscopy. The lipid water distribution coefficients of the GBP-based polypyridine metal complexes were calculated according to the following formula:

$$P = C_0/C_w$$

in which, C_0 represents the concentration of GBP-based polypyridine metal complex in the n-octanol phase, and C_w represents the concentration of GBP-based polypyridine metal complex in the aqueous phase.

2.4. Light-dark stability

The solutions of the synthesized GBP-based polypyridine metal complexes were placed under the dark condition for 24 h, and absorption spectrum before and after this period were recorded to evaluate their dark stability. Light stability of the synthesized GBP-based polypyridine metal complexes were analyzed by monitoring changes of absorption spectrum with the extension of visible light irradiation time.

2.5. Photodissociation efficiency

Photodissociation efficiency of the synthesized GBP-based polypyridine metal complexes were analyzed by UV–vis spectrophotometer. 5 mg of the synthesized GBP-based polypyridine metal complexes were singly dissolved in 10 mL DMSO to create 5 μg/mL solutions. The complex 1, 2, 3 and 4 solutions were individually irradiated under light at 231, 484, 478 and 400 nm for 1, 2, 3, 4, 5, 10, 30, 50, and 100 min. Then, the absorbance of the synthesized GBP-based polypyridine metal complexes were separately measured using the UV–vis spectrophotometer at each time interval. The same procedure was carried out for the GBP groups. The ratio of the absorbance obtained after a certain time and the initial absorbance was recorded.

2.6. Light-controlled antitumor activity and mechanism

2.6.1. Cell viability determination

The effect of the synthesized GBP-based polypyridine metal complexes on the cell viability of HN-3 cells and HELF cells were evaluated by methyl thiazolyl tetrazolium (MTT) method. Firstly, logarithmic HN-3 tumor cells (3.0×10^4 cells/mL) and HELF cells (2.8×10^4 cells/mL) suspensions were singly prepared and inoculated to 96-well plate (100 μL/well). The 96-well plate was placed in

an incubator with 37 °C and 5 % CO_2 for 24 h. Then, the synthesized GBP-based polypyridine metal complexes with different concentrations (5, 10, 15, 20, 25 μg/mL) were individually added into the plate, and incubated for 24 h under visible light irradiation. 50 μL of MTT solution (2 mg/mL) was added to incubate for 2 h, then the supernatant was poured out and 100 μL dimercaptosuccinic acid was added. After 20 s of oscillation, the absorbance at 540 nm was measured. The cell viability was calculated by the following formula: Cell viability (%) = average absorbance in the treatment group/average absorbance in the control group × 100 %.

2.6.2. ROS production capacity

The intracellular ROS levels of the synthesized GBP-based polypyridine metal complexes were qualitatively assessed by the DCFH-DA fluorescent probe. Firstly, the logarithmic HN-3 cells were digested, counted, and suspended at a density of 2×10^4 cells/mL. Subsequently, 200 μL of cell suspension (1×10^4 per well) was seeded into each well of the 24-well plate, incubated at 37 °C and 5 % CO_2 for 24 h, and then the corresponding complex containing medium was added. The negative control group was also included. After 24 h of complex treatment, the medium was replaced with fresh medium containing 10 μM DCFH-DA and incubated for 30 min. After visible light irradiation for 30 min, cells were washed three times with PBS. DAPI was diluted, added to the cells, incubated in dark for 20 min, and washed with phosphate buffer solution (PBS) three times. Finally, 1 mL of PBS was added to observe the experiment with a confocal microscope, and then three bright fields of view were taken and saved.

2.6.3. Cell apoptosis observation

The logarithmic HN-3 cells were digested, counted, and suspended at a density of 3×10^4 cells/mL. Subsequently, 200 μL of cell suspension (1×10^4 per well) was seeded into each well of the 24-well plate, incubated at 37 °C and 5 % CO_2 for 24 h, and then the corresponding complex containing medium was added. The negative control group was also included. After 24 h of complex treatment under visible light irradiation, An appropriate amount of PI staining solution (1:1000 dilution) and Hoechst 33,342 staining solution (1:1000 dilution) were added and placed at room temperature in dark for 20 min, then washed with PBS three times. Finally, 1 mL of PBS was added to observe the experiment with a confocal microscope, and then three bright fields of view were taken and saved.

2.6.4. Western blot analysis

Logarithmic HN-3 cells cultured in adherent culture were digested and extracted by total protein extraction kit to get total protein. The protein concentration was determined by BCA protein assay kit (Beyotime Biotechnology, China). SDS-PAGE and Western blotting were performed on the same amount of proteins according to the established method, where the primary antibodies were anti-Rabbit nuclear factor kappa-light-chainenhancer of activated B cells (NF-kB p-p65), B-cell lymphoma 2 (BCL-2) and BCL-2-associated X (BAX), as well as Rabbit Anti-β-actin (1:2000 or 1:5000 dilutions, Abcam, Inc.). Western blotting signals were observed using a G:BOX chemiXR5 imaging (SYNGENE, UK).

2.7. Light-controlled antibacterial activity and mechanism

2.7.1. Light-controlled antibacterial activity

The light-controlled antibacterial activity of the synthesized GBP-based polypyridine metal complexes against *S. aureus* were carried out using the method with minor modifications as described by Zhao et al. [19]. Each specimen was sterilized at 121 °C for 30 min by high-pressure steam sterilizer before the experiment. The *S. aureus* were cultivated in a nutrient broth medium at 37 °C for 18 h, and the final concentration of *S. aureus* was 1.2×10^9 colony forming units (CFU/mL). 100 μL of suspension of *S. aureus* was separately pipetted with a sterile pipette before coated on the Mueller-Hinton agar. After the bacterial suspension was fully permeated into the media, three sterilized oxford cups were evenly placed in a Petri dish with sterile forceps. Then, 100 μL of previously prepared complex solutions (3.0 mg/mL) were directly added separately to oxford cups, and Gentamycin sulfate (GS, 0.5 mg/mL) was served as a positive control. The culture dishes were placed in the dark and under the visible light irradiation respectively at 30 °C for a period of time so as to observe the antibacterial effect of each sample and measure the diameters of the inhibition zone with a vernier caliper.

The minimum inhibitory concentration (MIC) and the minimum bactericidal concentration (MBC) of the synthesized complexes were detected with the modified method proposed by Araujo et al. [20]. 100 μL of nutrient broth was pipetted into every well of 96-well microtitration plate. Then 100 μL of the synthesized complexes (3.0 mg/mL) and GS (0.5 mg/mL) were transferred into the first row of micro-titre plates. These solutions were separately diluted (two-fold dilutions) in nutrient broth. At last, 100 μL of *S. aureus* (adjusted to 0.5 McFarland, approximately 10^8 CFU/mL) was added in each well. All of the micro-titre plates were incubated in the dark and under the visible light irradiation respectively at 37 °C for 24 h. The MIC values were determined as the lowest concentration inhibiting the growth of bacteria. After broth microdilution tests, a 10 μL of sample was pipetted from wells and subcultured on new agar nutrient plates under 37 °C for 24 h in order to observe possible microbial development and also determine MBC values of the synthesized complexes.

2.7.2. The effect of complexes on bacterial cell walls

The collected logarithmic *S. aureus* were firstly washed with 0.1 M PBS buffer solution (pH = 7.2) and resuspended with the PBS buffer solution to 1×10^7 CFU/mL bacterial suspension, then the complexes were added and solutions with final concentrations of 0.5

× MIC, 1 × MIC, 2 × MIC were respectively achieved. The solutions were placed in a shaker under the visible light irradiation, and centrifuged at 4 °C for 10 min after being treated for 0, 2, 4, 6, 8, and 10 h. The contents of alkaline phosphatase (AKP) in the supernatant were measured according to the instructions of the kit, and the effect of the complexes on the bacterial cell walls were reflected based on the changes in AKP content.

2.7.3. The effect of complexes on bacterial cell membrane permeability

The collected logarithmic *S. aureus* were firstly washed with 5 % glucose solution and resuspended with the glucose solution to 1 × 10^7 CFU/mL bacterial suspension, making its conductivity value almost equal to that of 5 % glucose solution. Then the complexes were added, solutions with final concentrations of 0.5 × MIC, 1 × MIC, 2 × MIC were individually gained, and their conductivity values (L_1) were immediately measured. The solutions were placed under the visible light irradiation in a shaker at 4 °C, and their conductivity values (L_2) were measured after being treated for 0.5 h, 1 h, 2 h, 4 h, 6 h and 8 h. After the experiment was completed, a certain amount of bacterial suspension from the blank group was took out and placed in the boiling water for 10 min. After cooling, its conductivity (L_0) was recorded. In addition, the conductivity (L_0) of 5 % glucose solution was detected. The calculation method for relative conductivity was as follows: relative conductivity (%)=(L_2-L_1)/(L_0-L_0) × 100 %.

2.7.4. The effect of complexes on bacterial inclusion leakage

Leakage of bacterial inclusion contains leakage of nucleic acids and soluble proteins. Firstly, leakage of nucleic acids assay was conducted as follows: The collected logarithmic *S. aureus* were firstly washed with 0.1 M PBS buffer solution (pH = 7.2) and resuspended with the PBS buffer solution to 1 × 10^7 CFU/mL bacterial suspension, then the complexes were added and solutions with final concentrations of 0.5 × MIC, 1 × MIC, 2 × MIC were singly obtained; The solutions were placed under the visible light irradiation in a shaker at 4 °C for 8 h, then 5 mL of the solution was sucked up at room temperature and centrifuged for 10 min; Taking the supernatant and measuring the absorbance values at 260 nm and 280 nm, respectively. Leakage of soluble proteins assay was executed as following: Coomassie Brilliant Blue method was utilized to determine the soluble protein content in the supernatant.

2.7.5. SEM observation

The bacterial precipitates of *S. aureus* cultured until the logarithmic growth stage were centrifuged and collected, and diluted with fresh NB medium to 1 × 10^7 CFU/mL. The complexes were separately added, and solutions with final concentration of 1 × MIC and 2 × MIC were acquired. The solutions were incubated under the visible light irradiation at 37 °C for 8 h, and the bacterial bodies were gathered. Afterwards, the samples were prepared according to the sample processing requirements for scanning electron microscopy (SEM).

3. Results and discussion

3.1. Characterization results of GBP-based polypyridine metal complexes

The characterization result (see Fig. 5) of GBP-based polypyridine metal complex 1 was as follows: ^{1}H NMR (400 MHz, $CDCl_3$), δ: 8.42 (d, J = 8.6 Hz, 2H), 8.08 (d, J = 38.3 Hz, 6H) (pyrimidine, pyridine, C–Ir ortho hydrogen), 7.71 (d, J = 40.8 Hz, 13H), 7.30 (d, J = 7.4 Hz, 2H), 6.87 (d, J = 7.8 Hz, 2H), 6.69 (d, J = 8.5 Hz, 2H), 6.46 (t, J = 7.5 Hz, 2H), 6.19 (t, J = 7.9 Hz, 2H) (hydrogen on the benzene ring of the complex), 5.45 (br-t, =C<u>H</u>–CH_2–O, J = 6.8, 13.6 Hz, 1H), 5.12 (s, =CH, 38H), 4.07 (br-d, O–CH_2, J = 7.6 Hz, 52H), 1.89–2.10 (m, –CH_2, 155H), 1.75 (br-s, α-*cis*-CH_3, 95H), 1.68 (br-s, *cis*-CH_3, 257H), 1.63 (br-s, *trans*-CH_3, 86H). From above data of ^{1}H NMR, it was concluded that the complex 1 was sucessfully synthesized. In addition, the iridium content of the complex 1 was calculated as 1.52 % (m/m) by inductively coupled plasma (ICP) method.

The characterization result (see Fig. 6) of GBP-based polypyridine metal complex 2 was as following: ^{1}H NMR (400 MHz, $CDCl_3$), δ: 8.42 (d, J = 8.7 Hz, 1H) (hydrogen on pyridine ring), 8.19–7.93 (m, 4H) (pyridine and C–Ir ortho hydrogen), 7.77–7.47 (m, 9H), 7.00 (s, 1H), 6.87 (d, J = 7.5 Hz, 1H), 6.70 (t, J = 7.1 Hz, 2H), 6.45 (d, J = 7.3 Hz, 1H), 6.19 (t, J = 8.1 Hz, 1H) (other hydrogen on the complex), 5.48 (br-t, J = 33.2 Hz, =C<u>H</u>–CH_2–O, 1H), 5.13 (s, =CH, 29H), 4.04 (br-d, J = 7.6 Hz, O–CH_2, 32H), 2.04–2.10 (s, –CH_2, 88H), 1.75 (br-s, α-*cis*-CH_3, 63H), 1.68 (br-s, *cis*-CH_3, 96H), 1.59 (m, *trans*-CH_3, 100H). From above data of ^{1}H NMR, it was obvious that the complex 2 was sucessfully synthesized. Moreover, the iridium content of the complex 2 was computed as 1.68 % (m/m) by ICP method.

The characterization result (see Fig. 7) of GBP-based polypyridine metal complex 3 was as follows: ^{1}H NMR (400 MHz, $CDCl_3$), δ: 9.07 (dd, J = 16.0, 7.6 Hz, 1H), 8.89 (dd, J = 46.3, 8.5 Hz, 2H) (hydrogen on pyridine ring), 8.38 (d, J = 33.0 Hz, 4H) (pyridine and C–Ir ortho hydrogen), 8.20–7.85 (m, 11H), 7.60 (d, J = 41.6 Hz, 10H), 7.23–7.01 (m, 5H), 6.64 (s, 1H), 6.34 (s, 1H) (hydrogen on the benzene ring of the complex), 5.34 (s, =C<u>H</u>–CH_2–O, 1H), 5.12 (s, =CH, 17H), 4.12 (br-d, J = 7.2 Hz, O–CH_2, 48H), 1.97–2.04 (s, –CH_2, 54H), 1.62 (d, J = 41.6 Hz, 78H) (hydrogen on methyl group), 1.83 (br-s, α-*cis*-CH_3, 20H), 1.68 (br-s, *cis*-CH_3, 30H), 1.25 (br-s, *trans*-CH_3, 28H). From above data of ^{1}H NMR, it was proved that the complex 3 was sucessfully synthesized. Besides, the iridium content of the complex 3 was determined as 1.03 % (m/m) by ICP method.

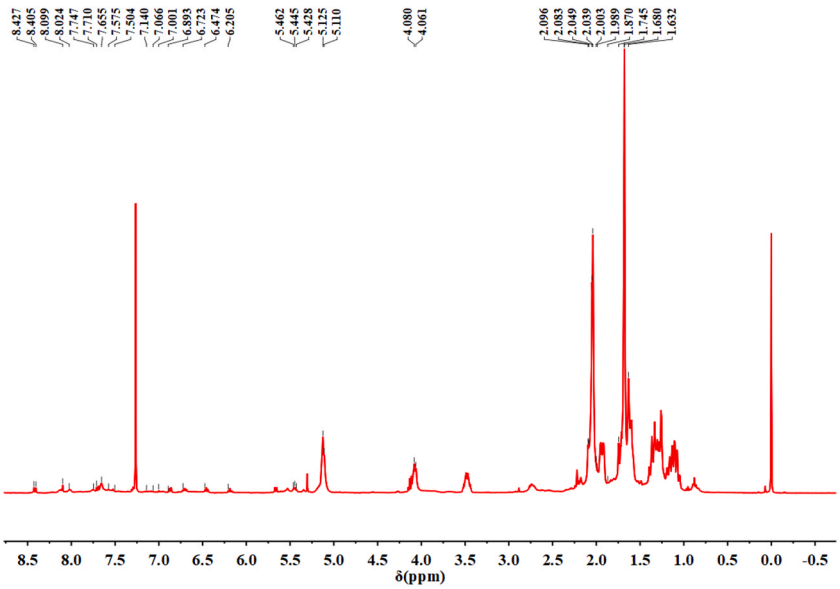

Fig. 5. ^{1}H NMR spectra of GBP-based polypyridine metal complex 1.

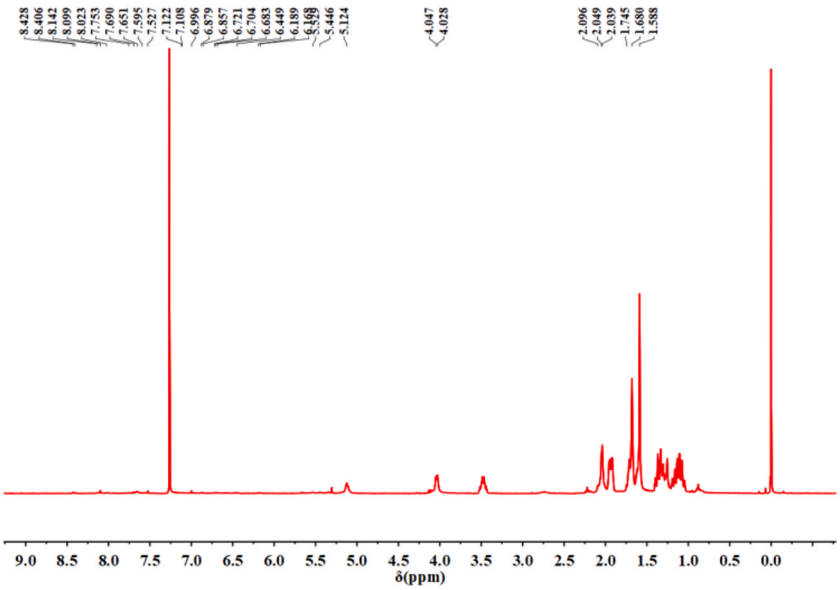

Fig. 6. ^{1}H NMR spectra of GBP-based polypyridine metal complex 2.

The characterization result (see Fig. 8) of GBP-based polypyridine metal complex 4 was as following: ^{1}H NMR (400 MHz, $CDCl_3$) δ: 8.84 (d, J = 6.3 Hz, 2H), 8.70 (d, J = 9.3 Hz, 1H), 8.66 (d, J = 11.0 Hz, 1H), 8.59 (d, J = 7.1 Hz, 1H), 8.25 (d, J = 10.1 Hz, 1H), 8.21–8.16 (m, 2H), 8.15–8.10 (m, 2H), 8.09–8.02 (m, 2H), 8.01–7.97 (m, 2H), 7.91 (t, J = 7.5 Hz, 1H), 7.71 (dd, J = 14.1, 5.1 Hz, 4H), 7.66–7.63 (m, 1H), 7.58–7.54 (m, 2H), 7.52–7.47 (m, 1H), 7.44 (s, 1H), 7.40–7.36 (m, 2H) (hydrogen on aromatic rings), 5.60 (br-t, =C<u>H</u>–CH_2–O, J = 7.1 Hz, 1H), 5.14 (s, =CH, 15H), 5.05 (d, O–CH_2, J = 8.5 Hz, 2H), 2.06 (s, α-*cis*-CH_3, 50H), 1.60 (s, *trans*-CH_3, 60H). From above data of ^{1}H NMR, it was sure that the complex 4 was sucessfully synthesized. Furthemore, the ruthenium content of the complex 4 was calculated as 1.25 % (m/m) by ICP method.

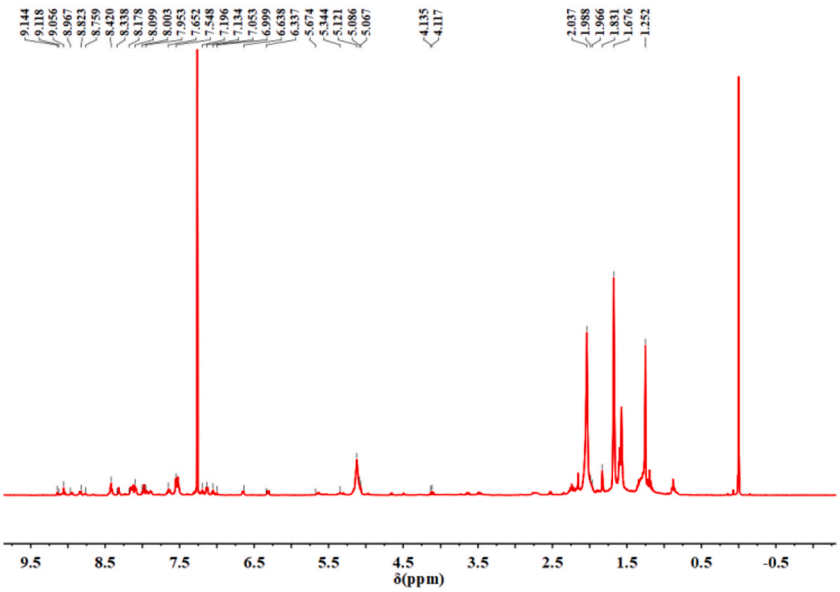

Fig. 7. ^{1}H NMR spectra of GBP-based polypyridine metal complex 3.

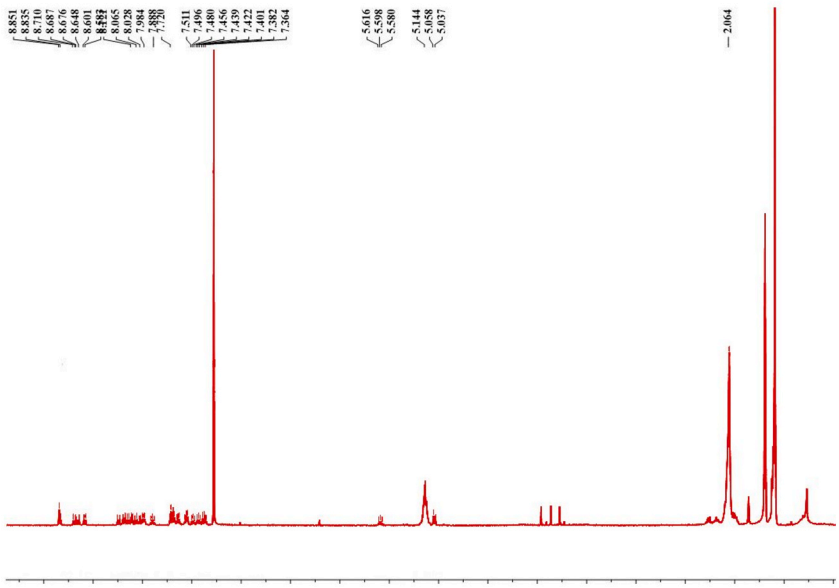

Fig. 8. ^{1}H NMR spectra of GBP-based polypyridine metal complex 4.

3.2. Analysis of cell absorption capacity

The detection results of lipid water partition coefficients for the complex 1, 2, 3 and 4 were demonstrated in Table 1. It was reported that when the lipid water partition coefficient of a compound between 0 and 3, its hydrophilicity and lipophilicity was optimal and most suitable for penetrating cell membrane [21]. Therefore, when the synthesized complexes possess appropriate lipid water partition coefficients, they will also exhibit potential of excellent bioavailability. It was obvious that the lipid water distribution coefficients of

Table 1
Lipid water partition coefficients of the synthesized metal complexes.

	Complex 1	Complex 2	Complex 3	Complex 4	GBP
Lipid water partition coefficients	2.45	1.82	3.56	1.56	5.86

complex 1, 2 and 4 were all within the range of 0~3, illustrating that they owned outstanding bioavailability properties. The complex 3 was not within the range of 0~3, but its hydrophilicity was greatly improved compared with GBP. The relatively high hydrophobicity of GBP makes it difficult to penetrate cell membrane, thereby resulting in its low bioavailability. After the chemical modification, the hydrophilicity of the synthesized complexes were all reformed, with the order of complex 4>complex 2>complex 1>complex 3>GBP.

3.3. Evaluation of light-dark stability

Dark stability is very vital for the application of polypyridine metal complexes. The absorption spectra changes of the complex 1, 2, 3, and 4 under darkness were exhibited in Fig. 9. From Fig. 9, it can be seen that the absorption spectra of the complex 1, 2, 3 and 4 presented almost no changes after being placed under dark condition for 24 h, indicating that all of the four synthesized GBP-based metal complexes possessed excellent dark stability. The absorption spectra changes of the complex 1, 2, 3 and 4 under the condition of visible light irradiation were demonstrated in Fig. 9. It was obvious that the complex 1 displayed little variation, while complex 2, 3 and 4 respectively emerged isoabsorption points at 484 nm, 478 nm and 400 nm, this indicated that the three complexes gradually underwent ligand dissociation with the extension of visible light irradiation time.

3.4. Analysis of photodissociation efficiency

Photodynamic degradation rate was adopted to reflect the photodissociation efficiency of the synthesized complexes under visible light irradiation, and related results were manifested in Fig. 10. From Fig. 10, it can be seen that the relative absorption intensity of complex 1 and GBP presented no changes, proving that they were very stability under visible light irradiation. Complex 2 (238 nm and 484 nm), complex 3 (374 nm and 478 nm) and complex 4 (262 nm and 400 nm) had two absorption peaks in their absorption spectra,

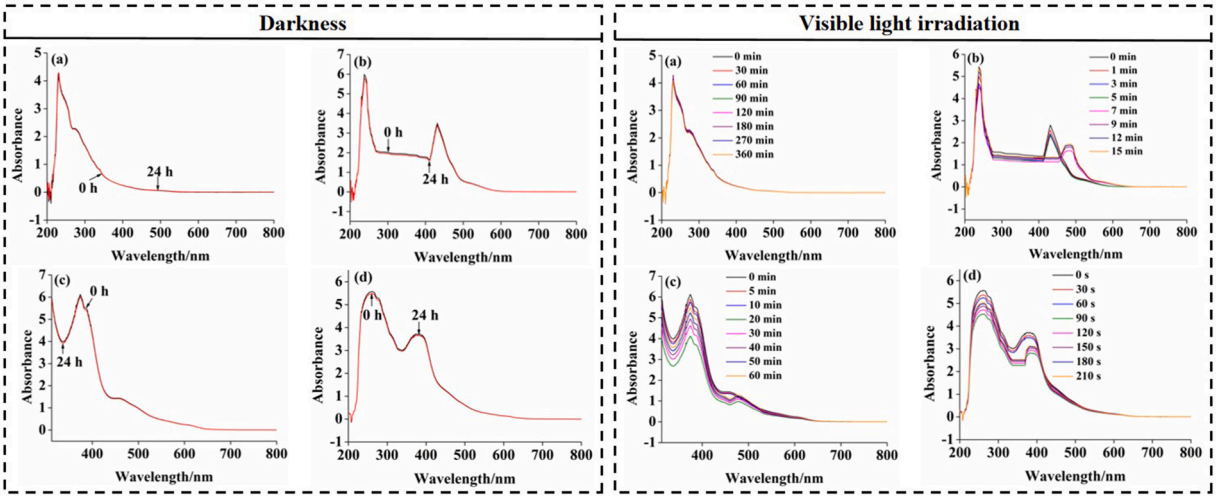

Fig. 9. Absorption spectra changes of complex 1(a), 2 (b), 3 (c), and 4 (d) under the condition of darkness and visible light irradiation.

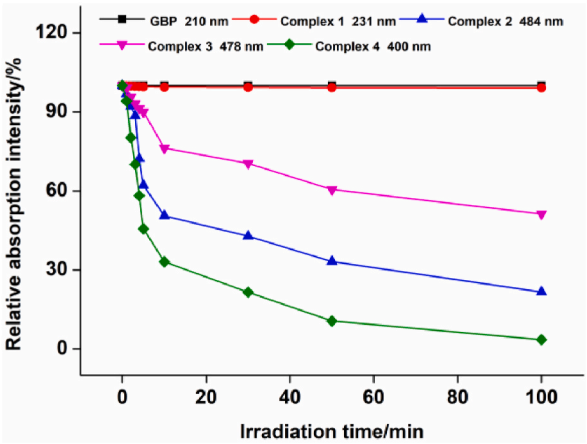

Fig. 10. Photodynamic degradation rates of the synthesized complexes under visible light irradiation.

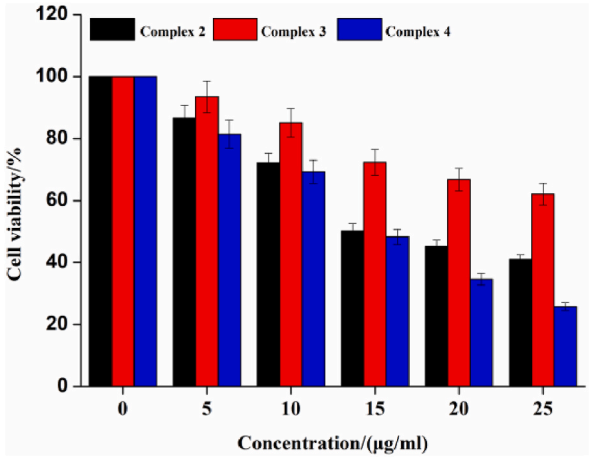

Fig. 11. Cell viability analysis of the complexes under light irradiation.

but the relative absorption intensity of complex 2, 3 and 4 appeared no variation at 238 nm, 374 nm and 262 nm, respectively. Therefore, 484 nm, 478 nm and 400 nm were singly utilized to analysis the photodynamic degradation rates of complex 2, 3 and 4. It was obvious that complex 2, 3 and 4 performed degradation with the visible light irradiation time increasing, in which complex 2 and complex 4 were able to achieve degradation rates of 37.9 % and 54.4 % within 5 min, separately.

According to the results of degradation rates, the order of photodissociation efficiency was complex 4>complex 2>complex 3>complex 1. This proved that the substituent group of the hydroxyl at the end of GBP may be related to the ligand dissociation efficiency of their metal polypyridine complexes. It was generally believed that the photodissociation efficiency of the complex was positively correlated with the escape rate of the two generated fragment molecules from the solvent cage. Therefore, the water solubility of the fragment molecules may produce a certain impact. However, based on the hydrophilicity order of the four synthesized complexes determined earlier, this study found that their ligand dissociation efficiency order was inconsistent with their hydrophilicity order. This result indicated that the difference in water solubility alone cannot effectively explain the final effect of substituents. The ligand dissociation efficiency of the synthesized complexes may be related to various factors such as its electron absorption ability and coordination ability etc., and further in-depth research is needed in the future.

3.5. Results of light-controlled antitumor activity and mechanism

There is almost no effect on the cell viability of HELF cells, indicating that the synthesized complexes are non-toxic to normal cells. The effect of the synthesized complexes on the cell viability of HN-3 cells under light irradiation were exhibited in Fig. 11. It was found

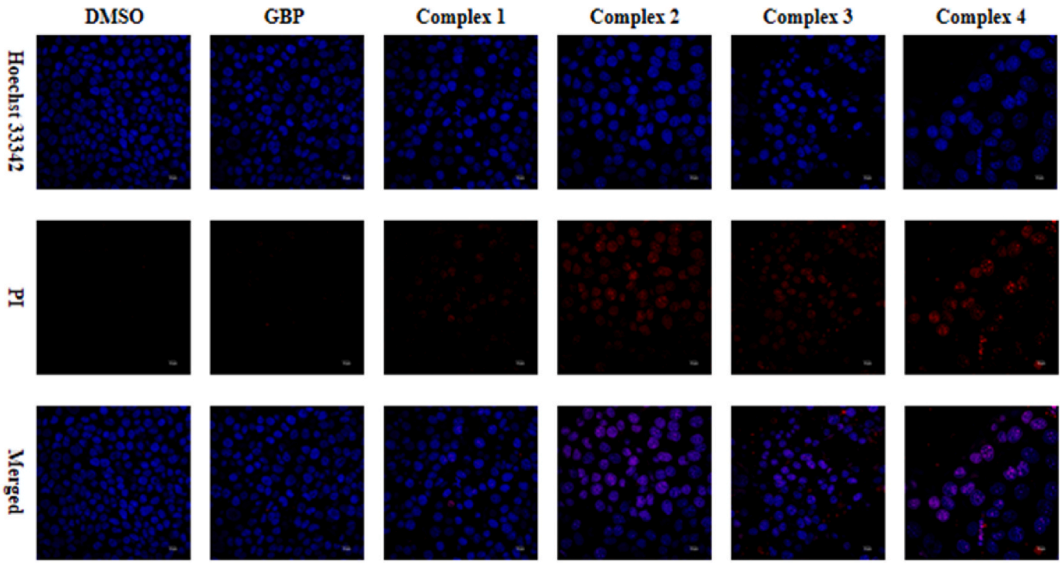

Fig. 12. Apoptosis induced by the synthesized complexes in HN-3 cells.

that both GBP and complex 1 demonstrated no influence on the cell viability of HN-3 cells, while complex 2, 3 and 4 displayed strong inhibitory effect on the cell viability of HN-3 cells. This may be because that GBP itself possessed no inhibitory effect on the cell viability of HN-3 cells, while chemical modified complex 1 could not realize ligand dissociation and produce ROS under light irradiation, resulting in it was not able to constrict the cell viability of HN-3 cells. The effect of complex 2, 3 and 4 on the cell viability of HN-3 cells gradually strengthened with the enhancement of their concentrations. Complex 4 manifested the best inhibitory effect when the concentration was 25 μg/mL, and could reach up to 74.2 % of inhibition rate on the cell viability of HN-3 cells.

Hoechst 33,342 is a nucleic acid fluorescent dye. Normal cells stained with Hoechst 33,342 indicate blue circular nuclei, while apoptotic cells display bright blue nuclei that were wrinkled, densely stained, and sometimes fragmented. Fluorescent dye PI cannot penetrate the complete cell membrane, so normal cells and early apoptotic cells will not be stained. For late stage apoptotic and necrotic cells, PI can dye the nucleus purple red. Late stage apoptotic cells exhibit concentrated and fragmented nuclei stained with both purple and bright blue. Necrotizing cells appear as circular nuclei with purple and blue double staining. Apoptosis induced by the synthesized complexes in HN-3 cells were indicated in Fig. 12. As shown in Fig. 12, groups treated with Dimethyl sulfoxide (DMSO), GBP and complex 1 presented bright blue nuclei, and almost no purple red nuclei appeared. In the meantime, groups processed with complex 2, 3 and 4 emerged purple red nuclei, especially complex 2 and 4 appeared a large number of purple red nuclei. This also verified the good inhibitory effect of complex 2 and 4 on the cell viability of HN-3 cells.

ROS production capacity is an extremely important factor in reversing drug resistance. The fluorescent labeling dye H_2DCFDA (DCFH-DA) itself does not emit fluorescence and can be converted into DCFDA with green fluorescence after ROS oxidation [22]. Therefore, H_2DCFDA staining can indirectly reflect the strength of ROS generation. ROS generation induced by the synthesized complexes in HN-3 cells were demonstrated in Fig. 13. It can be seen from Fig. 13, groups treated with DMSO, GBP and complex 1 had no green fluorescence appeared, while groups processed with complex 2, 3 and 4 displayed green fluorescence, in particular complex 2 and 4 showed abundant green fluorescence. Thus, It was concluded that the ROS production capacity of the synthesized complexes

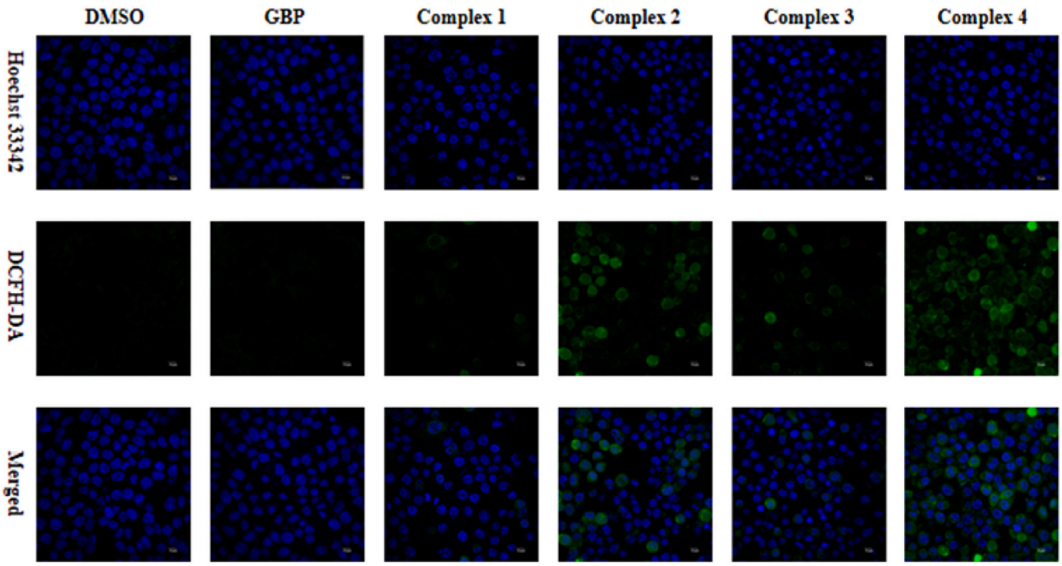

Fig. 13. ROS generation induced by the synthesized complexes in HN-3 cells.

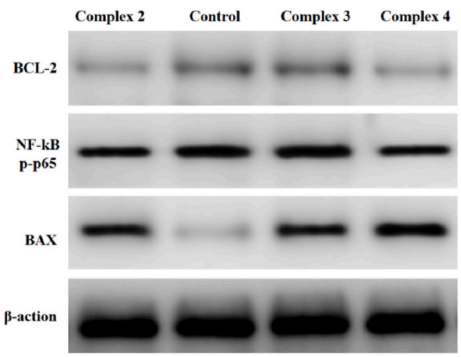

Fig. 14. The expression of apoptosis factors in HN-3 cells treated with the synthesized complexes.

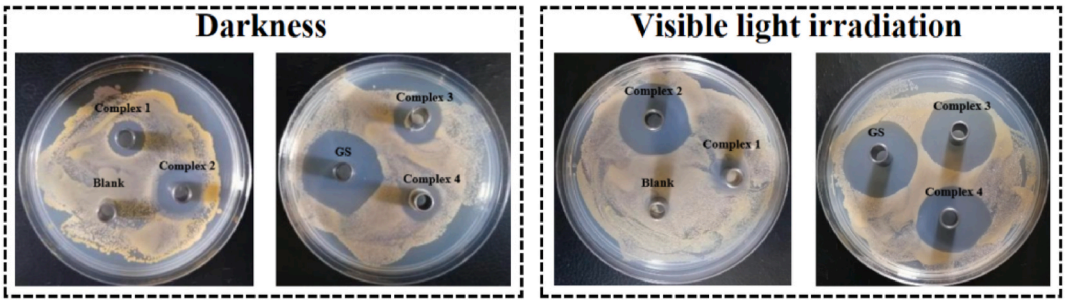

Fig. 15. Inhibition effects of the synthesized complexes against S. aureus under darkness and visible light irradiation.

possessed positive correlation with their inhibitory effect on the viability and apoptosis of HN-3 cells.

The protein expression changes of NF-kB p-p65, BCL-2 and BAX in HN-3 cells were analyzed by Western blot method after the co-incubation with the synthesized complexes, and β-actin was used as a reference, as shown in Fig. 14. Compared with blank control group, the pro-apoptotic protein factor BAX was evidently expressed and the expression of anti-apoptotic protein factor BCL-2 was inhibited in complex 2 and 4 groups. The highest expression of protein BAX was found in the complex 4 group, this result indicated that the complex 4 reinforced the apoptosis rate of HN-3 cells. Observably, there are some relationships between the expression of nuclear factor NF-kB p-p65 protein and BAX, which is attributed to the nature of nuclear factor NF-kB p-p65 protein that regulated the expression of apoptosis-related factors. Taken together, complex 2, 3 and 4 mainly induced apoptosis of HN-3 cells through BAX pathway.

3.6. results of light-controlled antibacterial activity and mechanism

The irrational use and even abuse of antibiotics produced a relatively serious antimicrobial resistance issue, which has become one of the most urgent global public health challenges [23]. Currently, photodynamic antibacterial is recognized as the main way to address antimicrobial resistance issue. This is because that it is a method of killing bacteria by combining photosensitizer molecules with ROS produced by visible light, ROS can react with various bioactive molecules in pathogenic bacteria, making them difficult to generate drug resistance [24]. The inhibition effects of the synthesized complexes against S. aureus were revealed in Fig. 15. As shown in Fig. 15, the antibacterial circle diameters of complex 2, 3 and 4 under visible light irradiation were significantly better than darkness, especially complex 4, while complex 1 presented little difference. The calculated results of MBC and MIC values for the synthesized complexes against S. aureus were unveiled in Table 2. Obviously, the MBC and MIC values of the synthesized complexes against S. aureus were 12.5–100 μg/mL and 6.25–50 μg/mL, respectively. In which, complex 4 exhibited the best antibacterial activity with MIC value of 6.25 μg/mL and MBC value of 12.5 μg/mL. The excellent antibacterial activity of complex 4 may be in connection with multiple factors, including the strongest ROS production capacity, photodissociation efficiency and cell absorption ability. Although complex 1 could not conduct ligand dissociation and possessed no ROS production capacity, it also showed certain inhibitory

Table 2
MBC and MIC values of the complexes under visible light irradiation.

	GS	Complex 1	Complex 2	Complex 3	Complex 4
MBC/(μg/mL)	8	100	25	50	12.5
MIC/(μg/mL)	4	50	12.5	25	6.25

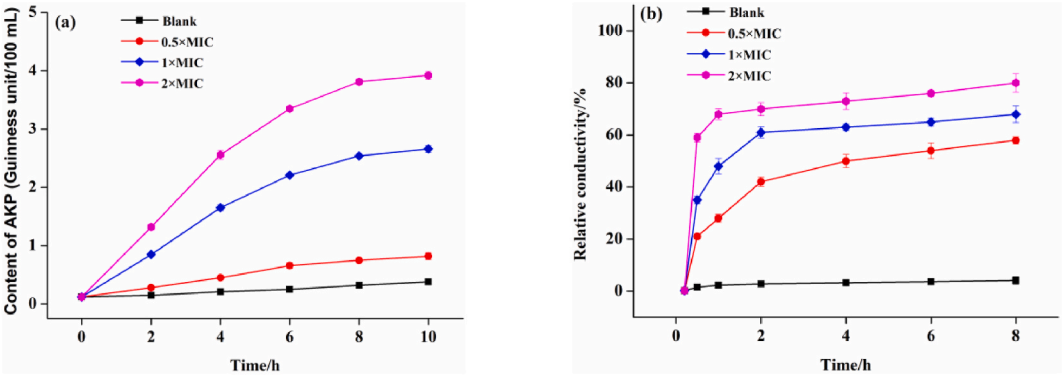

Fig. 16. Effect of the complex 4 on the cell wall (a) and cell membrane (b) of S. aureus

Table 3
Leakage of bacterial inclusion caused by complex 4.

Complex 4	Content of inclusion		
	OD260 nm	OD280 nm	Soluble protein/(μg/mL)
Blank	0.020 ± 0.001	0.015 ± 0.005	12.0 ± 1.1
0.5 × MIC	0.113 ± 0.021	0.105 ± 0.022	48.21 ± 3.0
1 × MIC	0.231 ± 0.050	0.153 ± 0.040	59.22 ± 4.3
2 × MIC	0.525 ± 0.062	0.432 ± 0.056	78.84 ± 5.4

effect against S. aureus, this was attributed to its own antibacterial activity. In order to study the antibacterial mechanism, complex 4 was selected as raw material in the subsequent experiments on account of its great potential in the field of efficient antibacterial agents.

The effect of the complex 4 on bacterial cell walls was shown in Fig. 16a it was obvious that the AKP content in the culture medium remained almost unchanged when no complex was added to culture with S. aureus. When 0.5 × MIC complex 4 was added, the content of AKP in the culture medium only increased slightly, with an increase of only 0.82 Guinness units/100 mL within 10 h. While the addition amount of the complex 4 improved to 1 × MIC and 2 × MIC, the AKP content in the culture medium significantly raised, and presented a significant enhancement within 6 h then demonstrated a relatively stable augment in the later stage. After 10 h of cultivation, the AKP content elevated by 2.66 and 3.96 Guinness units/100 mL, respectively. This indicated that the complex 4 could disrupt the cell wall integrity of S. aureus, leading to the outflow of AKP, and was able to cause damage to the cell wall in a short period of time.

The effect of complex 4 on bacterial cell membrane permeability was illustrated in Fig. 16b. As shown in Fig. 16b, when no complex was added to culture with S. aureus, the conductivity value of the bacterial suspension increased from 0.2 % at 0 h to 4.1 % at 8 h, with a small enhancement. While 0.5 × MIC, 1 × MIC and 2 × MIC complex 4 were added, the conductivity values of the bacterial suspension upgraded to 58 %, 68 %, and 80 %, respectively, and appeared remarkable augment within 0.5 h. These results explained that the concentration of conductive ions in the bacterial suspension gradually went up with the enhancement of the added complex 4 concentration. When the addition amount of the complex 4 reached 2 × MIC, most of the ions in S. aureus had already leaked out, indicating that the addition of complex 4 can damage the cell membrane of S. aureus in a short period of time, significantly improving the permeability of the cell membrane. Moreover, the higher the concentration of the complex 4, the stronger the permeability of the cell membrane.

The bacterial cell wall and cell membrane, as the external barriers of bacteria, play an important role in protecting bacteria and ensuring their normal growth. Once the bacterial wall membrane system is damaged, it can cause the leakage of many important biological macromolecules (such as nucleic acids, proteins, sugars, etc.) inside the bacteria, causing disruption in the normal synthesis and metabolism function of the bacteria. Therefore, the integrity of the bacterial wall membrane system can be reflected by measuring the changes in the content of substances that leak to extracellular space of cell. The results of bacterial inclusion leakage caused by the complex 4 were displayed in Table 3. As shown in Table 3, when no complex was added, the absorbance values and soluble protein contents of S. aureus supernatant at 260 and 280 nm were very low. When S. aureus was cultured with 0.5 × MIC complex 4 for 8 h, the soluble protein contents and absorbance values of the supernatant at 260 and 280 nm increased. After treatment with 1 × MIC and 2 × MIC complex 4, the absorbance values markedly improved. These results proved that wall and membrane system of S. aureus can be disrupted by complex 4, resulting in the leakage of large molecules within the cell.

The SEM results of S. aureus were exhibited in Fig. 17. As shown in Fig. 17, when not treated with complex 4, the morphology of S. aureus was intact, presenting a typical spherical shape, smooth and flat, with bright colors and good refractive index. There was no damage to the cell surface or any outflow of intracellular substances, and S. *aureus* grew well without aggregation. While being treated with 1 × MIC of complex 4, wrinkles and no filling sensation were found on the surface of the mycelium, and a small number of cells showed breakage and damage, resulting in rough surface of the mycelium. While being treated with 2 × MIC of complex 4, the surface roughness and wrinkling of the bacterial body became more severe, and the typical spherical shape of S. *aureus* could no longer be seen. At the same time, the leakage of cell inclusion intensified, and bacterial cells adhered and formed clusters due to the viscosity of the inclusion, resulting in serious overlap. This manifested that the complex 4 had destructive and damaging effect on S. aureus' cells, which can cause leakage of cell contents by forming pores on the cell wall and membrane. This also confirmed the changes in bacterial fluid conductivity, AKP and cell inclusion.

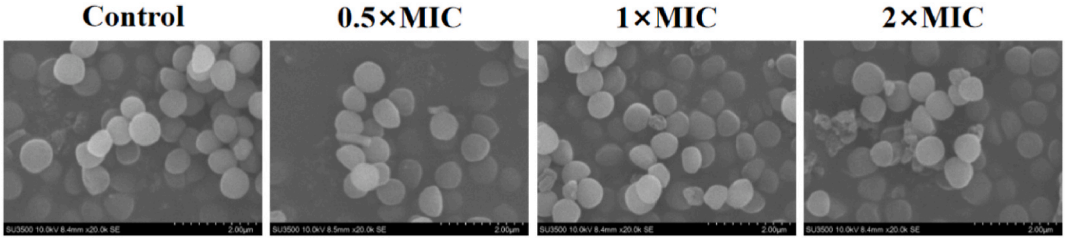

Fig. 17. SEM of S. aureus influenced by complex 4.

4. Conclusion

Four kinds of novel GBP-based polypyridine metal complexes were successfully synthesized, and possessed improved cell absorption capacity compared with GBP. All of the synthesized complexes had excellent dark stability and photoinduced ligand dissociation capacity except complex 1. Moreover, complex 2 and complex 4 exhibited superior inhibitory effect on the cell viability of HN-3 cells mainly by producing ROS and inducing cell apoptosis through BAX pathway. In addition, complex 4 demonstrated the best inhibitory activity against S. *aureus* under visible light irradiation by various reasons, including strong cell absorption capacity, fast photodissociation efficiency, as well as causing leakage of bacterial inclusion, change of cell membrane permeability and disruption of cell wall. The comprehensive research of this study will pave a way in solving the development and application of GBP-base functional products.

Data availability statement

Data associated with the study has not been deposited into a publicly available repository. Data are available from the corresponding author on reasonable request.

CRediT authorship contribution statement

Changwei Zhang: Writing – review & editing, Writing – original draft, Supervision, Project administration, Conceptualization. **Hua Yuan:** Software, Methodology, Investigation, Data curation. **Hong Shen:** Visualization, Resources, Methodology, Formal analysis. **Chengzhang Wang:** Writing – review & editing, Validation, Project administration, Funding acquisition.

Declaration of Competing interest

The authors declare that they have no known competing financial interests or personal relationships that could have appeared to influence the work reported in this paper.

Acknowledgments

The work supported by National Natural Science Foundation of China (32101473) and Guizhou Provincial Key Technology R&D Program (No.2023244).

Appendix A. . Supplementary data

Supplementary data to this article can be found online at https://doi.org/10.1016/j.heliyon.2024.e35479.

References

[1] C.W. Zhang, M.F. Li, Z.W. Qi, et al., The construction of a green and efficient system for the separation of polyprenols from *Ginkgo biloba* leaves, Process. Biochem. 100 (2021) 252–259, https://doi.org/10.1016/j.procbio.2020.10.013.
[2] R. Tao, C.Z. Wang, J.Z. Ye, et al., Antibacterial/antifungal activity and synergistic interactions between C_{70}-C_{120} polyprenol homologs from *Ginkgo biloba* L. leaves and the corresponding synthetic derivatives, Eur. Food. Res. Technol. 239 (4) (2014) 587–594, https://doi.org/10.1007/s00217-014-2254-4.
[3] R. Tao, C.Z. Wang, Y. Lu, et al., Characterization and cytotoxicity of polyprenol lipid and vitamin E-TPGS hybrid nanoparticles for betulinic acid and low-substituted hydroxyl fullerenol in MHCC97H and L02 Cells, Int. J. Nanomed. 15 (2020) 2733–2749, https://doi.org/10.2147/IJN.S249773.
[4] R. Tao, C.Z. Wang, J.Z. Ye, et al., Antibacterial activity of *Ginkgo biloba* leaves polyprenols nanoemulsion combination with antibiotics, Chem. Ind. For. Prod. 37 (1) (2017) 81–86, https://doi.org/10.3969/j.issn.0253-2417.2017.01.010.
[5] Y. Zhou, C.Z. Wang, Z.J. Li, Antibacterial activity of *Ginkgo biloba* polyprenols and their derivatives, Chem. Ind. For. Prod. 33 (4) (2013) 53–56, https://doi.org/10.3969/j.issn.0253-2417.2013.04.010.
[6] C.W. Zhang, M.F. Li, R. Tao, et al., Physiochemical property and antibacterial activity of formulation containing polyprenol extracted from *Ginkgo biloba* leaves, Ind. Crop. Prod. 147 (2020) 112213, https://doi.org/10.1016/j.indcrop.2020.112213.
[7] H. Yuan, C.W. Zhang, P. Zhou, et al., Preparation of polyprenol/poly(β-amino ester)/galactose targeted micelle carrier for enhancing cancer therapy, Arabian. J. Chem. 16 (5) (2023) 104679, https://doi.org/10.1016/j.arabjc.2023.104679.
[8] Q.X. Zhou, X.S. Wang, Advances in Ru (II)-based photoactivated chemotherapy agents, Acta. Chim. Sinica. 75 (2017) 49–59, https://doi.org/10.6023/A16090470.
[9] M.A. Sgambellone, A. David, R.N. Garner, et al., Cellular toxicity induced by the photorelease of a caged bioactive molecule: design of a potential dual-action Ru (II) complex, J. Am. Chem. Soc. 135 (2013) 11274–11282, https://doi.org/10.1021/ja4045604.
[10] R. Tao, C.Z. Wang, J.Z. Ye, et al., Synthesis and antibacterial activity of nitrogenated and haloid derivatives of *Ginkgo biloba* leaves polyprenol, Chem. Ind. For. Prod. 36 (6) (2016) 29–34, https://doi.org/10.3969/j.issn.0253-2417.2016.06.005.
[11] Y. Zheng, Q.X. Zhou, W.H. Li, et al., DNA photocleavage in anaerobic conditions by a Ru(II) complex: a new mechanism, Chem. Commun. 51 (2015) 428–430, https://doi.org/10.1039/c4cc06552b.
[12] L.Q. Song, P.H. Liu, X.S. Wang, et al., Synthesis of new Ruthenium (II) bipyridyl complexes and studies on their photophysical and photoelectrochemical properties, Chin. J. Chem. 21 (6) (2003) 644–649.
[13] W.H. Lei, X.S. Wang, Research progress in photodynamic antibacterial photosensitizers, Imaging. Sci. Photochem. 31 (5) (2013) 321–334, https://doi.org/10.7517/j.issn.1674-0475.2013.05.321.

[14] N.A. Smith, Photoactivatable Ru(II) Polypyridyl Complexes as Antibacterial Agents, University of Warwick, 2015, https://doi.org/10.1002/cjoc.20030210613. PhD thesis.
[15] C.A. Puckett, J.K. Barton, Methods to explore cellular uptake of ruthenium complexes, J. Am. Chem. Soc. 129 (1) (2007) 46–47, https://doi.org/10.1021/ja0677564.
[16] Y. Zheng, Ru Complexes with Dual Activity of Photodynamic Therapy and Photoactivated Chemotherapy and Their DNA Photodamage Mechanisms, University of Chinese Academy of Sciences, 2016. PhD thesis.
[17] P.L. Lam, G.L. Lu, K.M. Hon, et al., Development of ruthenium(II) complexes as topical antibiotics against methicillin resistant *Staphylococcus aureus*, Dalton. T. 43 (10) (2014) 3949–3957, https://doi.org/10.1039/c3dt52879k.
[18] M. Mariappan, R. Alagarsamy, A.P. Panneerselvam, et al., Synthesis, solvatochromism, photochemistry, DNA binding, photocleavage, cytotoxicity and molecular docking studies of a ruthenium(II) complex bearing photoactive subunit, J. Photoch. Photobio. A. 356 (2018) 617–626, https://doi.org/10.1016/j.jphotochem.2018.02.001.
[19] C.J. Zhao, B. Feng, Y.T. Li, et al., Preparation and antibacterial activity of titanium nanotubes loaded with Ag nanoparticles in the dark and under the UV light, Appl. Surf. Sci. 280 (2013) 8–14, https://doi.org/10.1016/j.apsusc.2013.04.057.
[20] F.M. Araujo, M.C.S.M. Dantas, L.S.E. Silva, et al., Antibacterial activity and chemical composition of the essential oil of *Croton heliotropiifolius* Kunth from Amargosa, Bahia, Brazil, Ind. Crops Prod. 105 (2017) 203–206, https://doi.org/10.1016/j.indcrop.2017.05.016.
[21] J. Li, S. Song, W. Huang, et al., Novel drug-drug salts of enoxacin with enhanced antibacterial activity: insights from solubility and lipid-water partition coefficient, J. Mol. Liq. 385 (2023) 122443, https://doi.org/10.1016/j.molliq.2023.122443.
[22] H. Shen, C.W. Zhang, C.Z. Wang, et al., Lutein-based pH and photo dual-responsive novel liposomes coated with Ce6 and PTX for tumor therapy, ACS Omega 8 (34) (2023) 31436–31449, https://doi.org/10.1021/acsomega.3c04228.
[23] A.G. Elliott, J.X. Huang, S. Neve, et al., An amphipathic peptide with antibiotic activity against multidrug-resistant Gram-negative bacteria, Nat. Commun. 11 (1) (2020) 3184, https://doi.org/10.1038/s41467-020-16950-x.
[24] S. Li, S. Cui, D. Yin, et al., Dual antibacterial activities of a chitosan-modified upconversion photodynamic therapy system against drug-resistant bacteria in deep tissue, Nanoscale 9 (11) (2017) 3912–3924, https://doi.org/10.1039/c6nr07188k.